Dual-anion Strategy Induces Dual Enhancement Towards Ultrashort Phase-Matching Wavelength in Deep-UV Transparent d^0 Transition Metal Oxyfluorides

Dongdong Chu[†,‡], Kewang Zhang[†,‡], Congwei Xie*[†,‡], Keith T Butler[§], Zhihua Yang[†,‡], Shilie Pan*[†,‡]

[†]Research Center for Crystal Materials; State Key Laboratory of Functional Materials and Devices for Special Environmental Conditions; Xinjiang Key Laboratory of Functional Crystal Materials; Xinjiang Technical Institute of Physics and Chemistry, Chinese Academy of Sciences, 40-1 South Beijing Road, Urumqi 830011, China.

[‡]Center of Materials Science and Optoelectronics Engineering, University of Chinese Academy of Sciences, Beijing 100049, China

[§]Department of Chemistry, University College London, Gordon Street, London, WC1H 0AJ, UK

ABSTRACT: The d^0 transition metal oxides are the most commonly used nonlinear optical (NLO) materials in visible light regions, however, the limited band gaps seriously hinder their application in ultraviolet (UV) and deep ultraviolet (DUV). Achieving double enhancement of band gap and birefringence by regulating anionic units helps to push their phase-matching (PM) wavelength into UV/DUV. Herein, started from the famous NLO template $LiNbO_3$, the "dual-anion strategy" is proposed to regulate $[NbO_{6-x}F_x]$ octahedrons, the predicted $Li_2Nb_2O_{6-x}F_{2x}\cdot(LiF)_y$ (x=1,2,4; y=0,2) exhibit dual-property magnification of wide band gap (3.82-6.26 eV,1~3 eV larger than $LiNbO_3$) and extraordinary birefringence (0.100-0.322, 1~4 times that of $LiNbO_3$) with strong second harmonic generation (SHG) of 2.6-6.2 × KDP. Remarkably, Li_2NbOF_5-I and $LiNbOF_4$-II afford record-breaking PM wavelength (λ_{PM}=209 nm) ever reported for d^0 transition metal oxyfluorides. Further analysis uncovers that the fluorinated modification of band edges and increase of octahedral anisotropy are the main reasons for enhanced PM ability.

The nature of anionic groups in inorganic materials is always associated with the performance of compounds[1-6]. Understanding the intrinsic mechanism of functional anionic units and developing an effective method to ameliorate their functionality offers a controllable way to design new generations of functional materials[7-14]. Nonlinear optical (NLO) materials, as a significant role in laser systems, have always been a spotlight with the implementation of anionic group regulation[15-21]. On the one hand, electrons can be approximately bounded to a certain local area during second harmonic generation (SHG), which makes anionic groups crucial to NLO performance.[22-23] On the other hand, commercially available NLO materials from ultraviolet (UV) to infrared (IR) region including $KBe_2BO_3F_2$ (KBBF)[24], β-BaB_2O_4 (BBO)[25], LiB_3O_5 (LBO)[26], KH_2PO_4 (KDP)[27], $LiNbO_3$ (LN)[28] and $KTiOPO_4$ (KTP)[29] have diverse anionic groups with multiple assembly structures, providing the possibilities for the controllability of their structures and performances[30-39]. Even though, it is still challenging to optimize diverse properties in one material, especially for UV and deep-UV (DUV) applications. For instance, the strong SHG response (d_{ij} > 0.39 pm/V) and a short absorption edge (E_g > 6.2 eV) are mutually conflicting, and a wide band gap usually corresponds to small birefringence (Δn)[40], making it hard to ensure the phase-matching (PM) ability in UV/DUV region(λ_{PM} < 200 or 400 nm).

The anionic groups containing d^0 transition metal with second-order Jahn-Teller (SOJT) distortions are one of the most commonly used NLO-active groups in visible light regions, the out-of-center distortions (e.g., NbO_6, TiO_6 in LN and KTP) arising from metal dπ-oxygen pπ orbital interactions are potential to induce non-centrosymmetric (NCS) structures and generate strong SHG intensities[41-44]. The SOJT distortion also leads to increased polarization anisotropy, making birefringence capable of better PM ability[45]. Extensive attempts including $Nb_2O_3(IO_3)_2(SO_4)$ (6×KDP, Δn = 0.22)[46], $LiZrTeO_6$ (2.5×KDP, Δn = 0.06)[47], $BaTeMo_2O_9$ (15×KDP)[48], $BaTeW_2O_9$ (12.5×KDP), $K(VO)_2O_2(IO_3)_3$ (20×KDP)[49], $BaNbO(IO_3)_5$ (14×KDP)[50] and $Cs_3Nb_5GeO_{16}$ (Δn = 0.19)[51] demonstrate success in the visible to IR region. However, the high distortion usually corresponds to limited band gaps, which seriously influences transparency in short wavelength regions[52-54]. For example, $LiNbO_3$ exhibits a large SHG response of 25 pm/V but is only transparent in 350 ~ 4500 nm[55-56]. Based on the electronegativity difference of anionic groups, many strategies have been proposed to manipulate the band gap[57-61], resulting in a series of wide bandgap compounds with d^0 transition metal, such as $K_5(NbOF_4)(NbF_7)_2$ (5.88 eV, 4×KDP, Δn=0.07 @ 546 nm)[61], ZrF_2SO_4(6.02 eV, 3.2×KDP, 0.074 @ 546 nm), HfF_2SO_4(> 6.53 eV, 2.5×KDP, 0.058 @ 546 nm)[60], $ZrOF_4H_2$ (> 6.53 eV, 2.2×KDP, 0.035@ 546 nm)[52]. However, regulations based

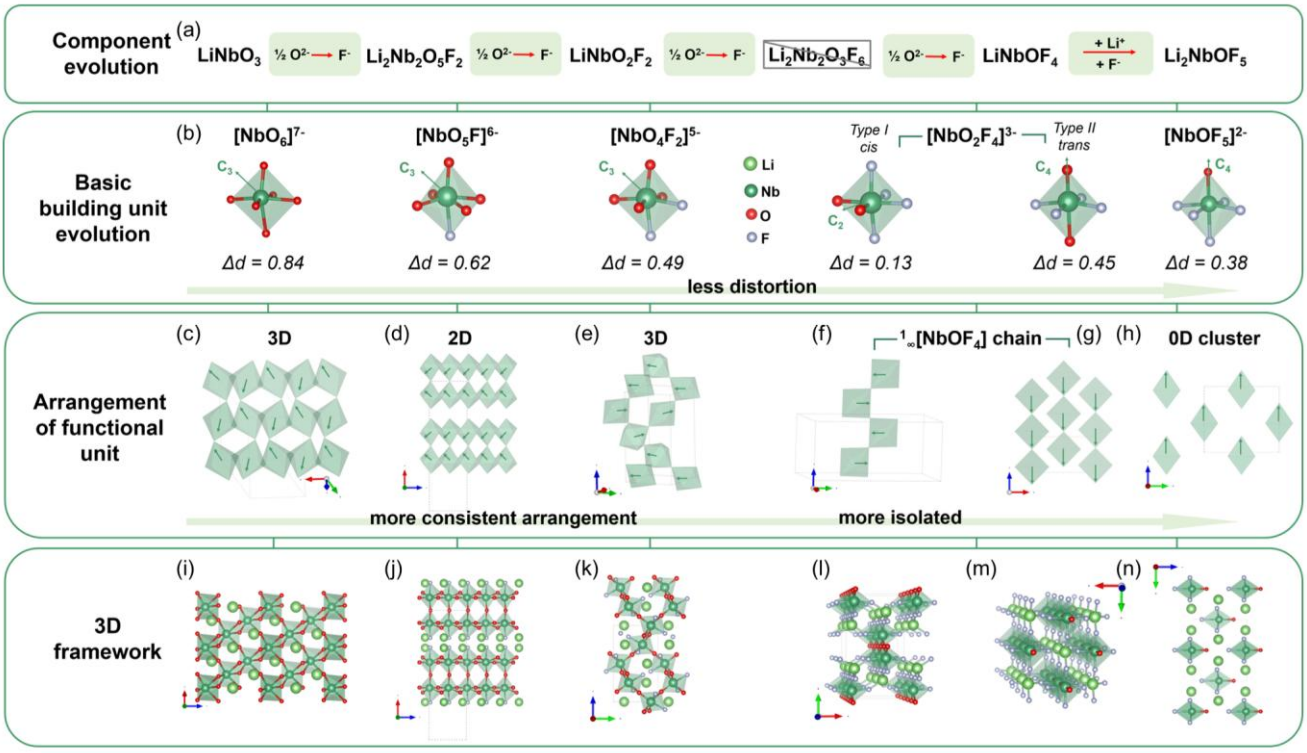

Figure 1. Structure descriptions of $LiNbO_3$ and $Li_2Nb_2O_{6-x}F_{2x}\cdot(LiF)_y$ (x=1, 2, 4; y=0, 2). (a) Component evolution from $LiNbO_3$ to Li_2NbOF_5 by dual-anion strategy. (b) Coordinate environments and the magnitude of the out-of-center distortion (Δd) of $[NbO_{6-x}F_x]^{(7-x)-}$ (x= 0, 1, 2, 4, 5) octahedron. (c-h) Arrangement of functional units, which shows lower degree of polymerization and more consistent arrangement with higher F/O ratio. (i-n) 3D structures of $LiNbO_3$, $Li_2Nb_2O_5F_2$-I, $LiNbO_2F_2$-I, $LiNbOF_4$-I, II and Li_2NbOF_5-I, respectively.

solely on adding large amounts of fluorine into a component leads to difficulties in controlling birefringence. Excessive introduction of fluorine will cause the d^0 transition metal to form polyhedral with multiple coordination, making it difficult to maintain octahedral configuration, which leads to non-parallel arrangements and results in relatively small birefringence (e.g. 0.035 and 0.026@546 nm for $ZrOF_4H_2$ and $HfOF_4H_2$), thus limiting the blueshift of their shortest PM wavelength. Therefore, in addition to enlarging the band gap, anisotropic anionic groups should also be taken into consideration. An efficient solution for this challenge lies in the introduction of two different anionic ligands, which proves a success especially in tetrahedral groups, contributing to the discovery of performance-enhanced UV/DUV NLO materials PNO[62], PNF_2[63], $SO_2(NH_2)_2$[64], $Sr(SO_3NH_2)_2$[65], etc. With central positive ions bonded to two anionic ligands (e.g., O, F, N, NH_2, *etc*.), the intrinsic polarizability anisotropy can be enhanced, further, by choosing the appropriate substituting anion, bandgap can also be improved. Such a dual-property enhancement will help to improve PM ability. However, there are very limited insights into this kind of anion modification in d^0 transition metal octahedron, let alone manipulating the properties through different ratios of two anion as well as regulating structures.

Herein, "dual-anion strategy" is proposed to adjust d^0 transition metal octahedron. Considering the high electronegativity, fluorine is chosen as a substitute for oxygen. To obtain large birefringence and SHG response by increasing the density of functional units while inducing orderly arrangement, small cations Li is chosen. Thus, the well-known $LiNbO_3$ with small size cation Li and NLO-active unit $[NbO_6]$ is chosen as a template. Eight thermodynamically stable/metastable structures $Li_2Nb_2O_{6-x}F_{2x}\cdot(LiF)_y$ (x=1, 2, 4; y=0,2) with different dual-anion ratios are predicted by component evolution design[66-67], exhibiting large band gap (3.82-6.26 eV) and birefringence (0.100-0.322) with strong SHG response of 2.6-6.2 × KDP. Remarkably, Li_2NbOF_5 can reach the DUV transparency (198 nm) with strong SHG response (2.6 × KDP), $Li_2Nb_2O_5F_2$-I and $LiNbOF_4$-II show extraordinary birefringence of 0.322 and 0.296 in UV region. In addition, the dual-anion strategy induces dual-property enhancement of band gaps (5.93, 6.25 eV) and birefringence (0.296, 0.167) in $LiNbOF_4$-II and Li_2NbOF_5-I, making them record-breaking in d^0 transition metal oxyfluorides with the shortest PM wavelength of 209 nm. Further in-depth mechanisms exploration demonstrates the effectiveness of our design strategy, uncovering that the fluorinated modification of band edges and the increase of octahedral anisotropy are the main reasons for the dual enhancement and thus better PM ability, which provides a new thought for the rational design of UV/DUV NLO materials.

Structure descriptions and NLO-related properties: Starting with $LiNbO_3$, a succinct and effective component evolution design as shown in Figure 1(a) is proposed for clarifying dual-anion strategy, by adjusting the ratio of dual-anion, the modified units should be $[NbO_{6-x}F_x]^{(7-x)-}$ (x= 1-5), and the

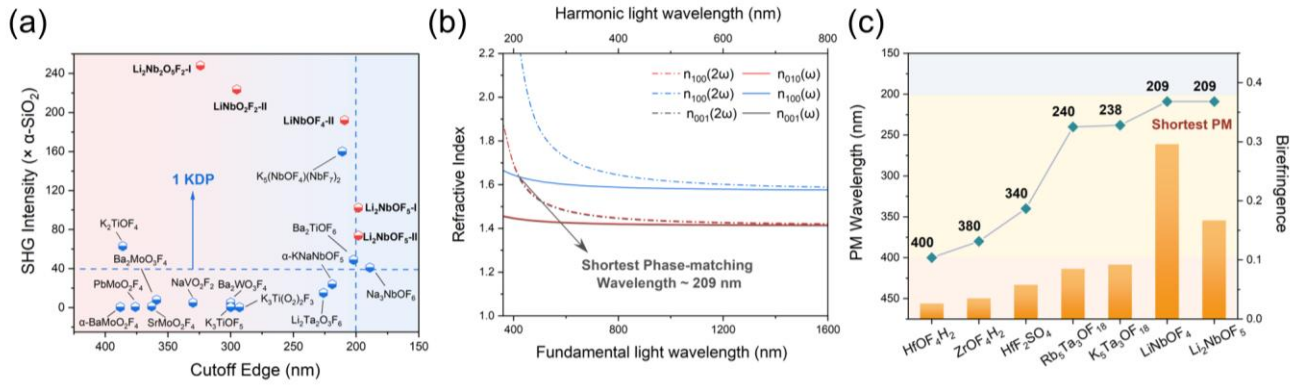

Figure 2. (a) The SHG intensity and cutoff edge of NCS $Li_2Nb_2O_5F_2$-I, $LiNbO_2F_2$-II, $LiNbOF_4$-II, and Li_2NbOF_5-I, II compared with some typical d^0-TM oxyfluorides (1×KDP≈40×SiO_2). (b) Refractive index dispersion curves and accordingly shortest PM wavelength of Li_2NbOF_5-I. (c) Birefringence and PM wavelength compared with other existing transition metal oxyfluorides.

variable components of the Li-Nb-O-F system can be $Li_2Nb_2O_{6-x}F_{2x}\cdot(LiF)_y$ (x=1, 2, 3, 4; y=0, 2). We systemically search the energetically favorable structures by USPEX and select the structures with E_{hull} < 10 meV. For each USPEX search, we performed three independent runs to increase the reliability of the predicted results. Among them, $Li_2Nb_2O_3F_6$ is dynamically unstable with imaginary phonon modes, other eight structures are identified with negative formation enthalpies and good dynamic stability (Figures S1-2), namely $Li_2Nb_2O_5F_2$-I, II; $LiNbO_2F_2$-I, II; $LiNbOF_4$-I, II and Li_2NbOF_5-I, II. To verify the credibility of our calculation, the structural rationality is also checked by suitable bond lengths and bond valence sum (BVS) as shown in Table S1, and all of the bond lengths are similar to existing niobium oxyfluorides such as $KNaNbOF_5$[68], $BaNbO(IO_3)_5$[50], $Sr_3Nb_2O_2F_{12}\cdot2H_2O$[69]. Remarkably, except for $LiNbOF_4$-I (Z=4) and $Li_2Nb_2O_5F_2$-II (Z=2) which crystallizes in centrosymmetric *Cmcm* (No.63) and *C*2/*m* (No.12), others all crystallize in NCS space groups $Cmc2_1$ (No.36), $P4_12_12$ (No. 92), $Pna2_1$ (No. 33), *Imm*2 (No. 44), *Imm*2 (No. 44), *Pc* (No. 7) for $Li_2Nb_2O_5F_2$-I (Z=4), $LiNbO_2F_2$-I (Z=4), II (Z=4); $LiNbOF_4$-II (Z=2), Li_2NbOF_5-I (Z=2), II (Z=2), respectively, indicating that Li-Nb-O-F may be a favorable system to explore potential NLO activity.

As is known to all, the basic building unit $[NbO_6]^{7-}$ in $LiNbO_3$ has always been regarded as a good NLO-active unit due to its strong face (C_3) distortion (Δd = 0.84). With anion regulation, four distinct building units $[NbO_{6-x}F_x]^{(7-x)-}$ (x= 1, 2, 4, 5) of the corresponding oxyfluorides $Li_2Nb_2O_{6-x}F_{2x}\cdot(LiF)_y$ (x=1, 2, 3, 4; y=0,2) are shown in Figure 1(b), all of the building units are experimentally observed in similar compounds, such as $Nb_{27}O_{54}F_{27}([NbO_5F])$[70], $NaNbO_2F_2([NbO_4F_2])$[71], $Rb_5Nb_3OF_{18}([NbO_2F_4])$[72], $KNaNbOF_5$ ($[NbOF_5]$)[68](Figure S8). With the increase of x, the $[NbO_{6-x}F_x]^{(7-x)-}$ (x= 1, 2, 4, 5) units gradually undergo the transition from face distortion (C_3) to edge distortion (C_2), and then to corner (C_4) distortion, in the meanwhile, the magnitude of the out-of-center distortion also decreases from 0.62-0.13 continuously. Different F/O ratio also results in different structure features. Compared with $LiNbO_3$, in which $[NbO_6]^{7-}$ unit rotates in two different directions (Figure 1(c)), and then connects with each other by corner-sharing O to form a 3D structure (Figure 1(i)), the increase in F/O ratio leads to overall "dimensional reduction" effect, making the 3D [NbO/F] framework ($LiNbO_3$, $LiNbO_2F_2$) collapses into 2D layer ($Li_2Nb_2O_5F_2$), 1D chain ($LiNbOF_4$) and 0D island-type connection (Li_2NbOF_5). In $LiNbO_2F_2$-I, corner-sharing $[NbO_4F_2]^{5-}$ rotate to reversed directions with the Nb-O-Nb angle of 160 ° to form a 3D structure as shown in Figure 1(e), the reversed arrangement and its crystallization in the D_4-422 point group leads to zero SHG coefficients, although it crystallizes in the NCS space group. As for $LiNbOF_4$-I and II, there are two types of $[NbO_2F_4]^{3-}$: type I cis- and type II trans-$[NbO_2F_4]^{3-}$units in the structures. The units share O atoms to form a 1D zigzag chain and straight chain, respectively (Figure 1(f-g)), each Li coordinates with four F to act as a chain-to-chain adhesive (Figure 1(l-m)). As for Li_2NbOF_5, its "zero-dimensional" (0D) anionic structure is composed of $[NbOF_5]^{2-}$ clusters arranged in the same direction along the c-axis (Figure 1(h)), with the Li^+ cations surrounded by one oxygen atoms and three F atoms to form $[LiOF_3]$ units, which acts as spacers between these anions (Figure 1(n)).

The key optical properties of $LiNbO_3$ and predicted compounds are listed in Table 1, $Li_2Nb_2O_5F_2$-I features the highest SHG responses of about 6.2 × KDP, Li_2NbOF_5-I features the lowest, but it can still reach the standard of 2.6 × KDP, indicating that Li-Nb-O-F is a very promising candidate system for NLO application. The band gaps of Li-Nb-O-F increase from 3.82 to 6.26 eV with higher dual-anion substitution, exhibiting a much wider transparency from UV to DUV compared with $LiNbO_3$ in visible region. Among them, Li_2NbOF_5-I and II reach DUV cutoff edge of 198 nm with strong SHG of 2.6 and 2.9 × KDP, acting as rare cases of DUV transparent d^0 transition metal oxyfluorides by theoretical design, exceeding the performance of $SrMoO_2F_4$, K_2TiOF_4, $NaVO_2F_2$, and α-$KNaNbOF_5$ (Figure 2(a)). Contrary to statistical intuition that band gaps and birefringence usually show opposite trends in the same system, our design of dual-anion d^0 metal octahedron shows a dual improvement in not only band gaps but also birefringence (0.100-0.322 @ 1064 nm). Remarkably, $Li_2Nb_2O_5F_2$-I and $LiNbOF_4$-II exhibit extraordinary birefringence of 0.322 and 0.296, which is close to that of α-$BaTeMo_2O_9$, and SbB_3O_6, far passing that of $LiNbO_3$, $CaCO_3$, and YVO_4 (Figure S3 and Table S4). The dual-property improvement makes $LiNbOF_4$-II and Li_2NbOF_5-I reach the shortest UV PM wavelength (209 nm) compared with other existing transition metal oxyfluorides to date (Figures 2(b-c) and S4). The good optical performance aroused our curiosity, why is the dual-anion strategy in d^0 transition metal octahedron able to exhibit dual amplification thus enhanced PM ability while maintaining strong SHG response? What is the impact of

different anion ratios on the performance? Inspired by these, the structure-property relationship including band gap, PM ability and SHG response is further investigated.

Table 1. Band gaps (E_g, in eV), UV cutoff edge (in nm), the SHG coefficients (d_{ij}, in pm/V), birefringence (Δn @ 1064 nm), and the shortest phase-matching wavelengths (λ_{PM}, in nm) for $Li_2Nb_2O_5F_2$-I, II; $LiNbO_2F_2$-I, II; $LiNbOF_4$-I, II and Li_2NbOF_5-I, II.

Compounds	Space group	Z	E_g-GGA (eV)	E_g-HSE06 (eV)	E_g-PBE0 (eV)	UV cutoff edge(nm)	Δn @1064nm	SHG coefficients (pm/V)	λ_{PM} (nm)
$LiNbO_3$	*R*3*c*	6	2.68	3.3*		350*	0.088*	d_{22}=2.1; d_{15}=-4.6; d_{33}=-25.2*	/
$Li_2Nb_2O_5F_2$-I	*Cmc*2$_1$	4	1.91	3.82	4.53	323	0.322	d_{15}=1.47; d_{24}=-2.42; d_{33}=2.11	306
$Li_2Nb_2O_5F_2$-II	*C*2/*m*	2	2.54	4.61	5.33	269	0.130	/	/
$LiNbO_2F_2$-I	*P*4$_1$2$_1$2	4	2.25	4.07	4.89	304	0.100	/	515
$LiNbO_2F_2$-II	*Pna*2$_1$	4	2.46	4.20	5.06	295	0.141	d_{15}=-0.85; d_{24}=-2.18; d_{33}=-0.25	455
$LiNbOF_4$-I	*Cmcm*	4	2.45	4.24	5.09	292	0.225	/	/
$LiNbOF_4$-II	*Imm*2	2	3.72	5.93	6.78	209	0.296	d_{15}=1.88; d_{24}=1.65; d_{33}=-0.69	209
Li_2NbOF_5-I	*Imm*2	2	3.96	6.25	6.94	198	0.167	d_{15}=-1.03; d_{24}=-0.93; d_{33}=1.00	209
Li_2NbOF_5-II	*Pc*	2	3.97	6.26	6.93	198	0.136	d_{11}=-0.46; d_{15}=0.75; d_{12}=-0.08; d_{13}=-0.37; d_{24}=-0.01; d_{33}=-1.15	228

The band gaps calculated by HSE06 are converted to UV cutoff edge.
* represents data from experiments[53]

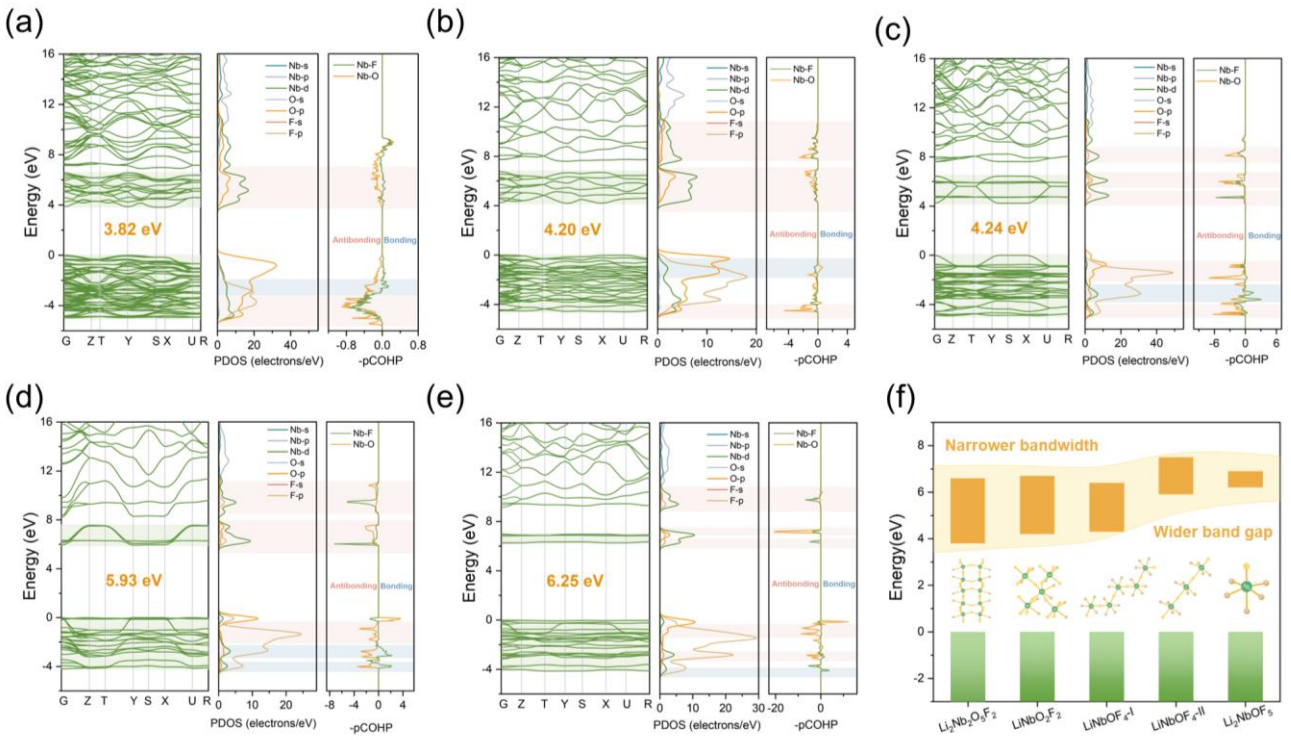

Figure 3. Calculated band structures, partial density of states (PDOS) and crystal orbital Hamilton population (COHP) of $Li_2Nb_2O_5F_2$-I (a), $LiNbO_2F_2$-II (b), $LiNbOF_4$-I (c), II (d), and Li_2NbOF_5-I (e). Pink and blue shades stand for anti-bonding and bonding states, green shades stand for bandwidth. (f) Schematic diagram of conduction band and valence band positions and widths of five Li-Nb-O-F.

Band-edge electronic features: To clarify the impact of our dual-anion strategy on the band edge, the band structure, partial density of states (PDOS) and underlying bonding properties (crystal orbital Hamilton population, COHP) of Li-Nb-O-F are further explored. The calculated band structure of $Li_2Nb_2O_5F_2$-I, $LiNbO_2F_2$-II, $LiNbOF_4$-I, II, and Li_2NbOF_5-I are shown in Figure 3(a-e), illustrating the dominating contribution of Nb-d, O-p and F-p in both the top of valence bands (VBM) and the bottom of conduction band (CBM), which exhibits distinctly different features with different ratios of dual-anion F/O. As the ratio increases, the bands in both VB and CB gradually flatten, especially for the CB part, which changes from highly curved bands ($Li_2Nb_2O_5F_2$, $LiNbO_2F_2$) to more flat bands ($LiNbOF_4$) and then turns to isolated intermediate bands (Li_2NbOF_5). Combined with PDOS and COHP analysis, CBM is mainly composed of Nb-O and Nb-F antibonding states, in which Nb-O antibonding gradually moves upward and exhibits more localized characteristics, leading to narrower bandwidth (Figure 3(f)) and higher anisotropy in CB, which are beneficial to enlarge the band gap and obtain high birefringence. For instance, as shown in Figure 3(c-d), the flat band of $LiNbOF_4$-I, II mainly originates from the antibonding hybridization and overlap of Nb-O and Nb-F, with higher F/O ratio, the Nb-O antibonding moves upward, and it shows less overlap with Nb-F anti-bond, resulting in the isolated intermediate bands in Li_2NbOF_5 [73-74](Figure 3(e)). As for the VB part, F-2p orbital gradually overwhelms O-2p, dominating the VB top from $Li_2Nb_2O_5F_2$ to Li_2NbOF_5, the F-2p orbitals show lower energy states thus widen the energy gap. Combined with COHP analysis, the VBM is mainly composed of Nb-O antibonding states, Nb-F and Nb-O bonding states, with the increase of F, the Nb-O antibonding orbital gradually upshift, while the Nb-O bonding states becomes more localized near the VBM, and Nb-F bonding orbital downshift to deeper energy region around -4 eV, which leads to narrower bandwidth, further enlarges the band gap.

In addition, structural factors also play an important role in band gaps, herein, the average band gaps of $LiNbO_2F_2$, $Li_2Nb_2O_5F_2$, $LiNbOF_4$, and Li_2NbOF_5 increase as the dimension of basic building units decreases from 3D to 0D (Figure S5). This difference can be inferred as the changes in atomic orbital connectivity induced by structure. As the structural dimensionality decreases from 3D to 1D, the connectivity of octahedron along the direction perpendicular to the chain breaks down, resulting in a lower connectivity of atomic orbitals, thus leading to reduced band dispersion and narrower bandwidths, which enlarges the band gap (Figure 3(c-d)). Similarly, the connectivity is further broken in 0D (Figure 3(e)), leading to even larger band gap, making Li_2NbOF_5-I, II as rare DUV transparent NLO candidates. It is worth noting that for $LiNbOF_4$-I-II with the same F/O ratio and 1D chain, their band gaps differ by almost 1.69 eV, indicating that the introducing straight chain formed by *trans*-[NbO_2F_4] is more beneficial to enlarge the band gap rather than zig-zag chain formed by *cis*-[NbO_2F_4]. The difference stems from the deeper F-2p orbitals in straight chain, which push the bonding state of Nb-F to deeper energy region around -4 eV as shown in Figure 3(c-d), thus widen the band gap. In conclusion, anion substitutions lead to a lower structural dimensionality in Li-Nb-O-F systems, which makes VB and CB to exhibit narrower bandwidth, drives Nb-O bonding states to become more localized and pushes Nb-F.

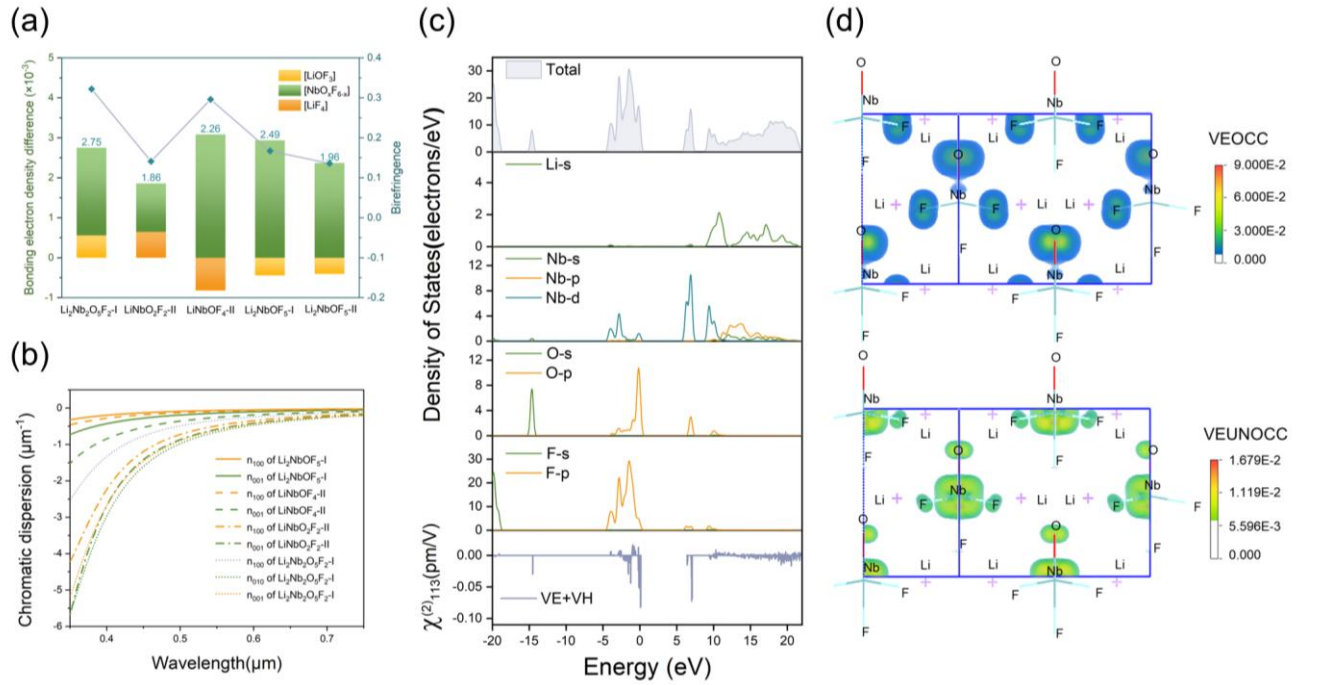

Figure 4. (a) Response electron distribution anisotropy (REDA) analysis of $Li_2Nb_2O_5F_2$-I, $LiNbO_2F_2$-II, $LiNbOF_4$-I, and Li_2NbOF_5-I, II respectively. (b) Chromatic dispersion characteristics of Li-Nb-O-F compounds, the refractive chromatic dispersion decreases continuously as the F/O increases. (c) Total and partial density of states and band-resolved SHG analysis of Li_2NbOF_5-I. (d) Occupied and unoccupied states of SHG density in the VE process of Li_2NbOF_5-I.

bonding orbital to deeper region in VB, thereby increasing the band gap.

Phase-matching ability mechanism: To effectively generate coherent light via the SHG process, one of the paramount important requirements is the PM condition, which refers to when the refractive index of the second harmonic wave is equal to the refractive index of the fundamental wave(Figure 2(b)). Our proposed strategy demonstrates a success in improving PM ability, $LiNbOF_4$-II and Li_2NbOF_5-I reach the shortest UV PM wavelength (209 nm) to date, the internal mechanism is worth exploring.

Previous studies reveal that the large birefringence and small refractive index chromatic dispersion (dn/dλ) have a significant effect on blueshift of PM wavelength.[75-77]In Li-Nb-O-F system, all compounds exhibit birefringence larger than 0.10, three of which can reach the birefringence over 0.2. To quantitatively analyze the contribution of the group to the birefringence, the response electron distribution anisotropy (REDA) method, which is proposed to analyze the relationship between optical anisotropy and chemical bonds, is adopted[78-79]. The bonding electron density difference $\Delta\rho^b$ of basic building units and corresponding birefringence of $Li_2Nb_2O_5F_2$-I, $LiNbO_2F_2$-II, $LiNbOF_4$-II and Li_2NbOF_5-I, II are shown in Figure 4(a). All of the $[NbO_{6-x}F_x]$ units contribute more than 50% to the birefringence, proving that they are birefringent-active. Among which, dual-anion groups with consistent alignment or reduced dimensionality (2D or 1D) are more conducive producing large birefringence. For instance, the 1D $[NbO_2F_4]$ straight chain exhibits the largest $\Delta\rho$ of 0.00308, domaining the large birefringence (0.296) of $LiNbOF_4$. Apart from birefringence, the refractive chromatic dispersion decreases continuously as the dual anion F/O ratio increases (Figure 4(b)), indicating the positive effect on optimizing chromatic dispersion of dual-anion octahedral chromophores. This can also explain why Li_2NbOF_5-I with much smaller birefringence can reach the same level of PM wavelength as $LiNbOF_4$-II. Also, Li_2NbOF_5-I and II exhibit similar bandgaps, however, Li_2NbOF_5-I exhibits shorter PM wavelength, the difference mainly stems from the smaller birefringence and larger refractive chromatic dispersion of Li_2NbOF_5-II (Figure S9). Consequently, by dual-anion strategy, the refractive index dispersion is reduced, and birefringence is enlarged, both of which contribute to the improvement of PM capabilities in $LiNbOF_4$-II and Li_2NbOF_5-I.

SHG ability mechanism: As the representative $Li_2Nb_2O_5F_2$-I, $LiNbO_2F_2$-II, $LiNbOF_4$-II and Li_2NbOF_5-I maintain strong SHG response, SHG-density method and band-resolved SHG calculations[80] are employed to explore the potential NLO-active groups. Band-resolved SHG calculations show that the VB's sharp region consists of Nb-*p*, O-*p* and F-*p*, whereas the CB consists of Nb-*d*, O-*p* and F-*p* (Figures 4(c) and S6) for all four compounds. The shape of the SHG density around Nb, O, and F atoms also reveal a clear contribution to the SHG coefficient in both occupied and unoccupied states as shown in Figures 4(d) and S7, indicating that $[NbO_5F]$, $[NbO_4F_2]$, $[NbO_2F_4]$, $[NbOF_5]$ unit could be referred as promising NLO-active units with large nonlinear susceptibilities in the UV/DUV region, together with their parallel alignment being thought to produce high nonlinear bulk susceptibilities.

Dual-anion VS fluorination strategy: In this work, to widen the band gap, fluorine is chosen as a substitute for oxygen, which makes dual-anion strategy proposed here similar to the previously reported fluorination strategy. It should be noted that commonly used fluorination strategy focuses on the modification of a whole compound, not on a specific anionic group.

Traditional fluorination strategy may increase the band gap but fail to ensure the enlargement of birefringence due to the excessive introduction of fluorine. Our proposed "dual-anion strategy" refers to the introduction of two different anionic ligands in specific groups. We not only focus on the modification of band edges, but also improvement of birefringence by modifying d^0 transition metal octahedral configuration with moderate distortion, such a double boost induces enhanced PM ability. Also, with the distorted octahedron, the strong SHG response is maintained. Further, proposed strategy provides a broad adjustability to other anions (N, P, NH_2, *etc.*), leading to tunable performances, which is desirable for future study.

In summary, a dual-anion strategy is proposed to regulate the d^0 transition metal octahedron and construct new niobium oxyfluoride by evolutionary algorithm. A series of $Li_2Nb_2O_{6-x}F_{2x}\cdot(LiF)_y$ (x=1, 2, 4; y=0,2) are discovered with strong SHG response (2.6-6.2× KDP), wide UV-DUV transparency (3.82-6.26 eV) and extraordinary birefringence (0.100-0.322), achieving dual enhancement compared with their original template $LiNbO_3$. Notably, $LiNbOF_4$-II and Li_2NbOF_5-I is record-breaking in d^0 transition metal oxyfluorides with the shortest PM wavelength of 209 nm. Further analysis reveals that the narrow bandwidth, high electronic anisotropy and optimized chromatic dispersion are reasons for improved PM ability, indicating that $[NbOF_5]^{2-}$ can be as a new DUV NLO-active and birefringent-active units. Our dual-anion strategy and structure-property exploration provide a good foundation for the future optimization of UV/DUV phase-matching d^0 transition metal oxyfluorides.

ASSOCIATED CONTENT

Supporting Information. Formation enthalpies and phonon spectrums of predicted compounds; birefringence of predicted compounds compared with other well-known birefringent materials; refractive index dispersion curves and accordingly predicted shortest phase-matching wavelength; relationship between average band gap and dimension; total and partial density of states and band-resolved SHG analysis; SHG density analysis; crystallographic structural data, bond lengths and bond valence sum; computational details. This material is available free of charge via the Internet at http://pubs.acs.org.

AUTHOR INFORMATION

Corresponding Author

* cwxie@ms.xjb.ac.cn
* slpan@ms.xjb.ac.cn

Author Contributions

All authors have given approval to the final version of the manuscript.

Notes

The authors declare no competing financial interest.

ACKNOWLEDGMENT

This work is supported by Acknowledgments This work is supported by the National Key Research and Development Program of China (2021YFB3601502), Key Research Program of Frontier Sciences, CAS (ZDBS-LY-SLH035), National Natural Science Foundation of China (22193044, 61835014, 22335007), Natural Science Foundation of Xinjiang (2021D01E05), CAS Project for Young Scientists in Basic Research (YSBR-024), Xinjiang Major Science and Technology Project (2021A01001),, Tianshan Basic Research Talents (2022TSYCJU0001).

REFERENCES

1. Guo, Q.; Qi, X. Z.; Zhang, L.; Gao, M.; Hu, S.; Zhou, W.; Zang, W.; Zhao, X.; Wang, J.; Yan, B.; Xu, M.; Wu, Y. K.; Eda, G.; Xiao, Z.; Yang, S. A.; Gou, H.; Feng, Y. P.; Guo, G. C.; Zhou, W.; Ren, X. F.; Qiu, C. W.; Pennycook, S. J.; Wee, A. T. S., Ultrathin Quantum Light Source with Van Der Waals $NbOCl_2$ Crystal. *Nature* **2023,** *613*, 53-59.
2. Hollingsworth, M. D., Crystal Engineering: from Structure to Function. *Science* **2002,** *295*, 2410-2413.
3. Mutailipu, M.; Poeppelmeier, K. R.; Pan, S., Borates: A Rich Source for Optical Materials. *Chem. Rev.* **2021,** *121*, 1130-1202.
4. Fang, Y.; Wang, F.; Wang, R.; Zhai, T.; Huang, F., 2D $NbOI_2$: A Chiral Semiconductor with Highly In-Plane Anisotropic Electrical and Optical Properties. *Adv. Mater.* **2021,** *33*, e2101505.
5. Lei, B. H.; Yang, Z.; Yu, H.; Cao, C.; Li, Z.; Hu, C.; Poeppelmeier, K. R.; Pan, S., Module-Guided Design Scheme for Deep-Ultraviolet Nonlinear Optical Materials. *J. Am. Chem. Soc.* **2018,** *140*, 10726-10733.
6. Yu, H.; Zhang, W.; Young, J.; Rondinelli, J. M.; Halasyamani, P. S., Design and Synthesis of the Beryllium-Free Deep-Ultraviolet Nonlinear Optical Material $Ba_3ZnB_5O_{10}PO_4$. *Adv. Mater.* **2015,** *27*, 7380–7385.
7. Butler, K. T.; Davies, D. W.; Cartwright, H.; Isayev, O.; Walsh, A., Machine Learning for Molecular and Materials Science. *Nature* **2018,** *559*, 547-555.
8. Luo, J.; Wang, X.; Li, S.; Liu, J.; Guo, Y.; Niu, G.; Yao, L.; Fu, Y.; Gao, L.; Dong, Q.; Zhao, C.; Leng, M.; Ma, F.; Liang, W.; Wang, L.; Jin, S.; Han, J.; Zhang, L.; Etheridge, J.; Wang, J.; Yan, Y.; Sargent, E. H.; Tang, J., Efficient and Stable Emission of Warm-white Light from Lead-free Halide Double Perovskites. *Nature* **2018,** *563*, 541-545.
9. Abdelwahab, I.; Tilmann, B.; Wu, Y.; Giovanni, D.; Verzhbitskiy, I.; Zhu, M.; Berté, R.; Xuan, F.; Menezes, L. d. S.; Eda, G.; Sum, T. C.; Quek, S. Y.; Maier, S. A.; Loh, K. P., Giant Second-harmonic Generation in Ferroelectric $NbOI_2$. *Nat. Photon.* **2022,** *16*, 644-650.
10. Yang, Y.; Xiao, Y.; Li, B.; Chen, Y.-G.; Guo, P.; Zhang, B.; Zhang, X.-M., Stereochemically Active Lone-Pair Containing Metal Substitution in Polar Axis toward a Giant Phase-Matchable Optical Nonlinear Silicate Crystal $Li_3(OH)PbSiO_4$. *J. Am. Chem. Soc.* **2023,** *145*, 22577-22583.
11. Tao, S.; Schmidt, I.; Brocks, G.; Jiang, J.; Tranca, I.; Meerholz, K.; Olthof, S., Absolute Energy Level Positions in Tin- and Lead-based Halide Perovskites. *Nat. Commun.* **2019,** *10*, 2560.
12. Chaudhary, K.; Tamagnone, M.; Rezaee, M.; Bediako, D. K.; Ambrosio, A.; Kim, P.; Capasso, F., Engineering Phonon Polaritons in Van Der Waals Heterostructures to Enhance In-plane Optical Anisotropy. *Sci. Adv.* **2019,** *5*, eaau7171.
13. Tudi, A.; Han, S.; Yang, Z.; Pan, S., Potential Optical Functional Crystals with Large Birefringence: Recent Advances and Future Prospects. *Coord. Chem. Rev.* **2022,** *459*, 214380.
14. Xie, H.; Li, Z.; Liu, Y.; Zhang, Y.; Uher, C.; Dravid, V. P.; Wolverton, C.; Kanatzidis, M. G., Silver Atom Off-Centering in Diamondoid Solid Solutions Causes Crystallographic Distortion and Suppresses Lattice Thermal Conductivity. *J. Am. Chem. Soc.* **2023,** *145*, 3211-3220.
15. Chen, C.; Wang, Y.; Wu, B.; Wu, K.; Zeng, W.; Yu, L., Design and Synthesis of An Ultraviolet-transparent Nonlinear Optical Crystal $Sr_2Be_2B_2O_7$. *Nature* **1995,** *373*, 322-324.
16. Eaton, D. F., Nonlinear Optical Materials. *Science* **1991,** *253*, 281-287.
17. Shi, G.; Wang, Y.; Zhang, F.; Zhang, B.; Yang, Z.; Hou, X.; Pan, S.; Poeppelmeier, K. R., Finding the Next Deep-Ultraviolet Nonlinear Optical Material: $NH_4B_4O_6F$. *J. Am. Chem. Soc.* **2017,** *139*, 10645-10648.

18. Zhang, Z.; Wang, Y.; Zhang, B.; Yang, Z.; Pan, S., Polar Fluorooxoborate, NaB_4O_6F: A Promising Material for Ionic Conduction and Nonlinear Optics. *Angew. Chem. Int. Ed.* **2018,** *57*, 6577-6581.
19. Halasyamani, P. S.; Rondinelli, J. M., The Must-have and Nice-to-have Experimental and Computational Requirements for Functional Frequency Doubling Deep-UV Crystals. *Nat. Commun.* **2018,** *9*, 2972.
20. Wu, M.; Tikhonov, E.; Tudi, A.; Kruglov, I.; Hou, X.; Xie, C.; Pan, S.; Yang, Z., Target‐Driven Design of Deep‐UV Nonlinear Optical Materials via Interpretable Machine Learning. *Adv. Mater.* **2023,** *35*, 2300848.
21. Qiu, H.; Li, F.; Li, Z.; Yang, Z.; Pan, S.; Mutailipu, M., Breaking the Inherent Interarrangement of $[B_3O_6]$ Clusters for Nonlinear Optics with Orbital Hybridization Enhancement. *J. Am. Chem. Soc.* **2023,** *145*, 24401-24407.
22. Chen, C.; Wu, Y.; Li, R., The Anionic Group Theory of the Non-linear Optical Effect and its Applications in the Development of New High-quality NLO Crystals in the Borate Series. *Int. Rev. Phys. Chem.* **2008,** *8*, 65-91.
23. Chen, C.-t.; Liu, G.-z., Recent Advances in Nonlinear Optical and Electro-Optical Materials. *Annu. Rev. Mater. Sci.* **1986,** *16*, 203-243.
24. Chen, C.; Xu, Z.; Deng, D.; Zhang, J.; Wong, G.; Wu, B.; Ye, N.; Tang, D., The Vacuum Ultraviolet Phase‐matching Characteristics of Nonlinear Optical $KBe_2BO_3F_2$ crystal. *Appl. Phys. Lett.* **1996,** *68*, 2930-2932.
25. Chen, C. T.; Wu, B. C.; Jiang, A. D.; You, G. M., A New-Type Ultraviolet SHG Crystal-β-BaB_2O_4. *Sci. Sin. B* **1985,** *28*, 235-243.
26. Chen, C. T.; Wu, Y. C.; Jiang, A. D.; Wu, B. C.; You, G. M.; Li, R. K.; Lin, S. J., New Nonlinear-Optical Crystal: LiB_3O_5. *J. Opt. Soc. Am. B* **1989,** *6*, 616-621.
27. Eimerl, D., Electro-Optic, Linear, and Nonlinear Optical Properties of KDP and its Isomorphs. *Ferroelectrics* **1987,** *72*, 397-441.
28. Boyd, G. D.; Miller, R. C.; Nassau, K.; Bond, W. L.; Savage, A., $LiNbO_3$: An Efficient Phase Matchable Nonlinear Optical Material. *Appl. Phys. Lett.* **1964,** *5*, 234-236.
29. Driscoll, T. A.; Hoffman, H. J.; Stone, R. E.; Perkins, P. E., Efficient Second-Harmonic Generation in KTP Crystals. *J. Opt. Soc. Am. B* **1986,** *3*, 683-686.
30. Jiao, J.; Zhang, M.; Pan, S., Aluminoborates as Nonlinear Optical Materials. *Angew. Chem. Int. Ed.* **2023,** *62*, e202217037.
31. Cheng, H.; Li, F.; Yang, Z.; Pan, S., $Na_4B_8O_9F_{10}$: A Deep-Ultraviolet Transparent Nonlinear Optical Fluorooxoborate with Unexpected Short Phase-Matching Wavelength Induced by Optimized Chromatic Dispersion. *Angew. Chem. Int. Ed.* **2022,** *61*, e202115669.
32. Wang, X. F.; Wang, Y.; Zhang, B. B.; Zhang, F. F.; Yang, Z. H.; Pan, S. L., CsB_4O_6F: A Congruent-Melting Deep-Ultraviolet Nonlinear Optical Material by Combining Superior Functional Units. *Angew. Chem. Int. Ed.* **2017,** *56*, 14119-14123.
33. Wang, Y.; Zhang, B.; Yang, Z.; Pan, S., Cation-Tuned Synthesis of Fluorooxoborates: Towards Optimal Deep-Ultraviolet Nonlinear Optical Materials. *Angew. Chem. Int. Ed.* **2018,** *57*, 2150-2154.
34. Mutailipu, M.; Zhang, M.; Zhang, B.; Wang, L.; Yang, Z.; Zhou, X.; Pan, S., $SrB_5O_7F_3$ Functionalized with $[B_5O_9F_3]^{6-}$ Chromophores: Accelerating the Rational Design of Deep-Ultraviolet Nonlinear Optical Materials. *Angew. Chem. Int. Ed.* **2018,** *57*, 6095-6099.
35. Zhang, J.; Wu, C.; Shi, H.; Xie, C.; Yang, Z.; Pan, S., An Interlinked Prediction-experiment Paradigm Discovering Deep-Ultraviolet Fluorooxoborates with Desired Optical Nonlinearity and Birefringence. *Matter* **2023,** *6*, 1188-1202.
36. Mutailipu, M.; Zhang, M.; Wu, H.; Yang, Z.; Shen, Y.; Sun, J.; Pan, S., $Ba_3Mg_3(BO_3)_3F_3$ Polymorphs with Reversible Phase Transition and High Performances as Ultraviolet Nonlinear Optical Materials. *Nat. Commun.* **2018,** *9*, 3089.
37. Ahmed, S.; Cheng, P. K.; Qiao, J.; Gao, W.; Saleque, A. M.; Al Subri Ivan, M. N.; Wang, T.; Alam, T. I.; Hani, S. U.; Guo, Z. L.; Yu, S. F.; Tsang, Y. H., Nonlinear Optical Activities in Two-Dimensional Gallium Sulfide: A Comprehensive Study. *ACS Nano* **2022,** *16*, 12390-12402.
38. Chen, J.; Chen, H.; Xu, F.; Cao, L.; Jiang, X.; Yang, S.; Sun, Y.; Zhao, X.; Lin, C.; Ye, N., $Mg_2In_3Si_2P_7$: A Quaternary Diamond-like Phosphide Infrared Nonlinear Optical Material Derived from $ZnGeP_2$. *J. Am. Chem. Soc.* **2021,** *143*, 10309-10316.
39. Taghizadeh, A.; Thygesen, K. S.; Pedersen, T. G., Two-Dimensional Materials with Giant Optical Nonlinearities near the Theoretical Upper Limit. *ACS Nano* **2021,** *15*, 7155-7167.
40. Liang, F.; Kang, L.; Lin, Z. S.; Wu, Y. C.; Chen, C. T., Analysis and Prediction of Mid-IR Nonlinear Optical Metal Sulfides with Diamond-like Structures. *Coord. Chem. Rev.* **2017,** *333*, 57-70.
41. Lu, H.; Gautier, R.; Donakowski, M. D.; Tran, T. T.; Edwards, B. W.; Nino, J. C.; Halasyamani, P. S.; Liu, Z.; Poeppelmeier, K. R., Nonlinear Active Materials: An Illustration of Controllable Phase Matchability. *J. Am. Chem. Soc.* **2013,** *135*, 11942-11950.
42. Wang, Y.; Nisbet, M. L.; Kamp, K. R.; Hiralal, E.; Gautier, R.; Halasyamani, P. S.; Poeppelmeier, K. R., Beyond π–π Stacking: Understanding Inversion Symmetry Breaking in Crystalline Racemates. *J. Am. Chem. Soc.* **2023,** *145*, 16879-16888.
43. Gautier, R.; Gautier, R.; Chang, K. B.; Poeppelmeier, K. R., On the Origin of the Differences in Structure Directing Properties of Polar Metal Oxyfluoride $[MO_xF_{6-x}]^{2-}$ (x = 1, 2) Building Units. *Inorg. Chem.* **2015,** *54*, 1712-1719.
44. Halasyamani, P. S., Asymmetric Cation Coordination in Oxide Materials: Influence of Lone-Pair Cations on the Intra-octahedral Distortion in d^0 Transition Metals. *Chem. Mater.* **2004,** *16*, 3586-3592.
45. Wu, J.-H.; Hu, C.-L.; Jiang, T.-K.; Mao, J.-G.; Kong, F., Highly Birefringent d^0 Transition Metal Fluoroantimonite in the Mid Infrared Band: Order–Disorder Regulation by Cationic Size. *J. Am. Chem. Soc.* **2023**, https://doi.org/10.1021/jacs.3c09566.
46. Tang, H. X.; Zhang, Y. X.; Zhuo, C.; Fu, R. B.; Lin, H.; Ma, Z. J.; Wu, X. T., A Niobium Oxyiodate Sulfate with a Strong Second-Harmonic-Generation Response Built by Rational Multi-Component Design. *Angew. Chem. Int. Ed.* **2019,** *58*, 3824-3828.
47. Lu, W.; Gao, Z.; Liu, X.; Tian, X.; Wu, Q.; Li, C.; Sun, Y.; Liu, Y.; Tao, X., Rational Design of a $LiNbO_3$-like Nonlinear Optical Crystal, Li_2ZrTeO_6, with High Laser-Damage Threshold and Wide Mid-IR Transparency Window. *J. Am. Chem. Soc.* **2018,** *140*, 13089-13096.
48. Ra, H.-S.; Ok, K. M.; Halasyaman, P. S., Combining Second-Order Jahn-Teller Distorted Cations to Create Highly Efficient SHG Materials: Synthesis, Characterization, and NLO Properties of $BaTeM_2O_9$ (M = Mo^{6+} or W^{6+}). *J. Am. Chem. Soc.* **2003,** *125*, 7764-7765.
49. Yu, H.; Nisbet, M. L.; Poeppelmeier, K. R., Assisting the Effective Design of Polar Iodates with Early Transition-Metal Oxide Fluoride Anions. *J. Am. Chem. Soc.* **2018,** *140*, 8868-8876.
50. Chuan-Fu Sun, C.-L. H., Xiang Xu, Ji-Bei Ling, Ting Hu, Fang Kong, Xi-Fa Long, and Jiang-Gao Mao, $BaNbO(IO_3)_5$: A New Polar Material with a Very Large SHG Response. *J. Am. Chem. Soc* **2009,** *131*, 9486–9487.
51. Zhao, W.; Jiao, J.; She, Y.; Liang, F.; Ye, N.; Hu, Z.; Wu, Y.; Li, C., Tailored Ordered Structures with Functional Units of Distorted $[NbO_6]$ and Antiparallel $[GeO_4]$ for Enhanced Birefringence in Germanate Crystal. *Adv. Optical Mater.* **2022,** *10*, 2201704.
52 Jiang, C.; Jiang, X.; Wu, C.; Huang, Z.; Lin, Z.; Humphrey, M. G.; Zhang, C., Isoreticular Design of $KTiOPO_4$-Like Deep-Ultraviolet Transparent Materials Exhibiting Strong Second-Harmonic Generation. *J. Am. Chem. Soc.* **2022,** *144*, 20394-20399.
53 Hu, Y.; Wu, C.; Jiang, X.; Duanmu, K.; Huang, Z.; Lin, Z.; Humphrey, M. G.; Zhang, C., Ultrashort Phase‐Matching Wavelength and Strong Second‐Harmonic Generation in Deep‐UV‐Transparent Oxyfluorides by Covalency Reduction. *Angew. Chem. Int. Ed.* **2023**, *62*, e202315133.
54 Halasyamani, P. S.; Poeppelmeier, K. R., Noncentrosymmetric Oxides. *Chem. Mater.* **1998,** *10*, 2753-2769.
55. Fedotova, A.; Carletti, L.; Zilli, A.; Setzpfandt, F.; Staude, I.; Toma, A.; Finazzi, M.; De Angelis, C.; Pertsch, T.; Neshev, D. N.;

Celebrano, M., Lithium Niobate Meta-Optics. *ACS Photonics* **2022,** *9*, 3745-3763.
56. Nikogosyan, D. N., *Nonlinear Optical Crystals: A Complete Survey*. Springer Science & Business Media: New York, 2006.
57. Hu, Y.; Wu, C.; Jiang, X.; Wang, Z.; Huang, Z.; Lin, Z.; Long, X.; Humphrey, M. G.; Zhang, C., Giant Second-Harmonic Generation Response and Large Band Gap in the Partially Fluorinated Mid-Infrared Oxide $RbTeMo_2O_8F$. *J. Am. Chem. Soc.* **2021,** *143*, 12455-12459.
58. Zhou, J.; Wu, H.; Yu, H.; Jiang, S.; Hu, Z.; Wang, J.; Wu, Y.; Halasyamani, P. S., $BaF_2TeF_2(OH)_2$: A UV Nonlinear Optical Fluorotellurite Material Designed by Band-Gap Engineering. *J. Am. Chem. Soc* **2020,** *142*, 4616-4620.
59. Tang, G.; Ghosez, P.; Hong, J., Band-Edge Orbital Engineering of Perovskite Semiconductors for Optoelectronic Applications. *J. Phys. Chem. Lett.* **2021,** *12*, 4227-4239.
60. Wu, C.; Jiang, C.; Wei, G.; Jiang, X.; Wang, Z.; Lin, Z.; Huang, Z.; Humphrey, M. G.; Zhang, C., Toward Large Second-Harmonic Generation and Deep-UV Transparency in Strongly Electropositive Transition Metal Sulfates. *J. Am. Chem. Soc.* **2023,** *145*, 3040-3046.
61. Wu, T.; Jiang, X.; Wu, C.; Hu, Y.; Lin, Z.; Huang, Z.; Humphrey, M. G.; Zhang, C., Ultrawide Bandgap and Outstanding Second-Harmonic Generation Response by a Fluorine-Enrichment Strategy at a Transition-Metal Oxyfluoride Nonlinear Optical Material. *Angew. Chem. Int. Ed.* **2022,** *61*, e202203104.
62. Xie, C.; Tudi, A.; Oganov, A. R., PNO: A Promising Deep-UV Nonlinear Optical Material with the Largest Second Harmonic Generation Effect. *Chem. Commun.* **2022,** *58*, 12491-12494.
63. Kang, L.; Zhang, X.; Liang, F.; Lin, Z.; Huang, B., Poly(difluorophosphazene) as the First Deep‐Ultraviolet Nonlinear Optical Polymer: A First‐Principles Prediction. *Angew. Chem. Int. Ed.* **2019,** *58*, 10250-10254.
64. Tian, H.; Ye, N.; Luo, M., Sulfamide: A Promising Deep‐Ultraviolet Nonlinear Optical Crystal Assembled from Polar Covalent $[SO_2(NH_2)_2]$ Tetrahedra. *Angew. Chem. Int. Ed.* **2022,** *61*, e202200395.
65. Fan, H.; Ye, N.; Luo, M., New Functional Groups Design toward High Performance Ultraviolet Nonlinear Optical Materials. *Acc. Chem. Res.* **2023**, https://doi.org/10.1021/acs.accounts.3c00575.
66. Glass, C. W.; Oganov, A. R.; Hansen, N., USPEX—Evolutionary crystal structure prediction. *Computer Physics Communications* **2006,** *175*, 713-720.
67. Oganov, A. R.; Pickard, C. J.; Zhu, Q.; Needs, R. J., Structure Prediction Drives Materials Discovery. *Nat. Rev. Mater.* **2019,** *4*, 331-348.
68. Holland, M. C., Nenian; Rondinelli, James M.; Poeppelmeier, Kenneth R., Reconstructive Transitions from Rotations of Rigid Heteroanionic Polyhedra. *J. Am. Chem. Soc* **2016,** *138*, 11882-11889.
69. Ko, E.; Jo, H.; Ok, K. M., $Sr_2Nb_6O_{13}F_8{\cdot}4H_2O$ and $Sr_3Nb_2O_2F_{12}{\cdot}2H_2O$: A Variant of Three-Dimensional Tungsten Bronze and a Polar Molecular Oxide Fluoride. *Inorg. Chem.* **2021,** *60*, 7914-7921.
70. Dabachi, J.; Body, M.; Galven, C.; Boucher, F.; Legein, C., Preparation-Dependent Composition and O/F Ordering in NbO_2F and TaO_2F. *Inorg. Chem.* **2017,** *56*, 5219-5232.
71. Andersson, S.; Galy, J., The Crystal Structure of $NaNbO_2F_2$. *Acta Cryst.* **1969,** *B25*, 847-850.
72. Agulyanskii, A. I. Z., V.E.; Kuznetsov, V.Ya.; Sidorov, N.V.; Stefanovich, S.Yu.; Tsikaeva, D.V.; Kalinnikov, V.T., Structure and Some Properties of $Rb_5Nb_3OF_{18}$ Crystals. *Izvestiya Akademii Nauk SSSR, Neorganicheskie Materialy* **1991,** *27*, 1055-1060.
73. Ayer, G. B. a. K., Vladislav V. and Smith, Mark D. and Hu, Ming and Yang, Zhonghua and Martin, Corey R. and Morrison, Gregory and zur Loye, Hans-Conrad, $BaWO_2F_4$: A Mixed Anion X-ray Scintillator with Excellent Photoluminescence Quantum Efficiency. *Dalton Trans.* **2020,** *49*, 10734-10739.
74. Tang, G.; Xiao, Z.; Hong, J., Designing Two-Dimensional Properties in Three-Dimensional Halide Perovskites via Orbital Engineering. *J. Phys. Chem. Lett.* **2019,** *10*, 6688-6694.
75. Pan, X.; Liu, F.; Lin, Z.; Kang, L., Birefringent Dispersion Optimization to Achieve Superior Nonlinear Optical Phase Matching in Deeper Solar-Blind UV Band from KH2PO4 to BeH3PO5. *Small* **2023**, 2308811, https://doi.org/10.1002/smll.202308811.
76. Jiang, X.; Luo, S.; Kang, L.; Gong, P.; Huang, H.; Wang, S.; Lin, Z.; Chen, C., First-Principles Evaluation of the Alkali and/or Alkaline Earth Beryllium Borates in Deep Ultraviolet Nonlinear Optical Applications. *ACS Photonics* **2015,** *2*, 1183-1191.
77. Cheng, H.; Li, F.; Yang, Z.; Pan, S., $Na_4B_8O_9F_{10}$: A Deep-Ultraviolet Transparent Nonlinear Optical Fluorooxoborate with Unexpected Short Phase-Matching Wavelength Induced by Optimized Chromatic Dispersion. *Angew. Chem. Int. Ed.* **2022,** *61*, e202115669.
78 Lei, B. H.; Yang, Z.; Yu, H.; Cao, C.; Li, Z.; Hu, C.; Poeppelmeier, K. R.; Pan, S., Module-Guided Design Scheme for Deep-Ultraviolet Nonlinear Optical Materials. *J. Am. Chem. Soc.* **2018,** *140*, 10726-10733.
79 Lei, B. H.; Yang, Z.; Pan, S., Enhancing Optical Anisotropy of Crystals by Optimizing Bonding Electron Distribution in Anionic Groups. *Chem. Commun.* **2017,** *53*, 2818-2821.
80. Lee, M. H.; Yang, C. H.; Jan, J. H., Band-Resolved Analysis of Nonlinear Optical Properties of Crystalline and Molecular Materials. *Phys. Rev. B* **2004,** *70*, 235110.